Finite Element Analysis of Friction Stir Welding of Aluminum Alloy

Bijay Kumar Roy

Department of Mechanical Engineering/Jorhat Engineering College, Jorhat, Assam, India

Abstract: *Friction stir welding (FSW) is a relatively new joining process that is presently attracting considerable interest. The FSW process was developed at TWI (The welding institute) in 1991. Friction stir welding process is a solid-state joining process with the potential to join low melting point materials, particularly aluminum alloys. The surface finish of welded joint is very good in friction stir welding as compared with other welding process. In the present study, a finite element heat generation model in ABAQUS 6.14 was developed to estimate the amount of heat generation in friction stir welding of aluminum AA6061-T6 plate. The study was focused on numerical investigations for friction stir welding of aluminum AA6061-T6 plates. A 3-D finite element (FE) thermal analysis was carried out to determine the transient thermal profile during friction stir welding of aluminum alloy. The FSW tool was assumed as a heat source over the aluminum plates. Also, the effect of tool rotational speed and traverse speed on transient profiles was investigated.*

Key Word*: Friction stir welding (FSW), Transient thermal analysis, Finite element modelling, FSW Process parameters.*

I. Introduction

　　　Friction Stir Welding (FSW) is a solid-state welding method without using filler material. The process was invented by The Welding Institute (TWI), Cambridge, UK and patented in 1991 [1]. The process uses a spinning non-consumable tool to generate frictional heat in the work piece. FSW creates weld by the combined action of frictional heating and mechanical deformation, the maximum temperature reached is of the order of 0.8 of the melting temperature. It is being considered as a thermo-mechanical process which transforms heterogeneous microstructure of base metal to more homogeneous microstructure. The Friction Stir Welding Process is most suitable for critical applications, for the joining of structural components made of aluminum and its alloys. In Friction Stir Welding, a cylindrical-shouldered tool, with a profiled probe (nib or pin) is rotated at a constant speed and feed at a constant traverse rate into the joint line between two pieces of plates, butted together. The tool has a circular section except at the end where there is a probe; the junction between the cylindrical portion and the probe is known as the shoulder[2]. The heat is generated primarily by friction between a rotating and translating tool, the shoulder of which rubs against the work piece. It softens the material and enables the material plastic deformation [3, 4]. In the last decade a consistent work was performed on the numerical simulation of FSW in order to develop a proper numerical model able to aid the design process. A number of academic and industrial institutions have made efforts to develop numerical codes for FSW. Although FSW is simple in concept, the physics behind the process is complex, which includes mechanical heat generation, heat and mass transport. The large strains and strain rates make observing the details of the process difficult, which makes process modeling attractive or essential to understand it. Two main approaches were considered, namely the use of analytical models, reproducing the thermal flux generated during the process, and of thermo-mechanical simulations through FE models. One of the first attempts were made by Chao et al.[5] proposed numerical models taking into account the heat generated by both friction-forces and material deformation work. The implementation of proper thermal boundary condition for the backing plate (anvil) is critical for accurate simulation results[6, 7]. The FSW tool taper angle plays a crucial role on peak temperature. Gadakh et al.[8] observed that increasing the taper pin angle leads to decrease in peak temperature by numerical simulation. The FSW tool geometry governs the proper mixing of material and welding defects. Fujii et al.[9] observed a defect-free weld in soft alloys such as AA1050 with use of a columnar tool pin without any thread, while a triangular prism-shaped tool pin was appropriate for hard alloys such as AA5083. The material flow induced by the pin is important to achieve a cavity-free weld joint [10]. Zhao et al.[11] examined minimum defects in AA2014 with application of a threaded tapered pin. The larger tool shoulder diameter results in higher peak temperatures of the weld material during FSW[12]. A larger shoulder diameter provides greater contact area, resulting in higher frictional and mechanical work that leads to higher temperature[13]. Deng et al.[14] used solid-mechanics based finite element

---

method with adaptive meshing to simulate the friction stir welding process. Two different interface models with rate-independent material were used to study the material flow. The lesser tool traverse speed leads to increase the peak temperature of the welded plates[15, 16]. Zhang et al.[17] observed from numerical results that the shape of the equivalent plastic strain looks like onion rings and the spacing of the rings is approximately equal to the forward movement of the tool in one rotation. Ulysse[18] investigated the effect of tool speeds on the process parameters for FSW of aluminum plates using a FEM code and found a decrement in peak temperature with tool rotational speed. Nandan et al.[19] observed the asymmetry in the temperature profiles around the FSW tool because of the rotational and traverse speed of the tool and asymmetry heat generation in the vicinity of tool pin surface. Nandan, et al.[20] further expanded the study to mild steel. Although they claimed that the computed temperatures were in good agreement with the corresponding experimentally determined values, only temperatures at one remote point from the tool were reported. Chen et al.[21] investigated friction stir welding of aluminum alloy 2219-O and 2219-T6 to analyze the effects on the base material after FSW. The weld morphologies, weld defects, and mechanical properties of joints was observed after welding. The strength efficiency of 2219-O joints was found 100%, while that of 2219-T6 joints was only up to 82%. H.J. Liu et al.[22], conducted underwater friction stir welding on aluminum alloy 2219 to clarify the effect of varying welding speed while keeping the rotation speed fixed. The conclusion he got was that, tensile strength firstly increases with the welding speed but dramatically decreases at the welding speed of 200 mm/min owing to the occurrence of groove defect. Also, during tensile test, the joint welded at a lower welding speed is fractured in the heat affected zone on the retreating side. While at higher welding speed, the defect-free joint is fractured in the thermal mechanically affected zone on the advancing side. Weifeng Xu et al.[23], investigated temperature evolution, microstructure and mechanical properties of friction stir welded thick aluminum 2219-O joints. They observed dynamic recrystallized structures in the weld nugget zone (WNZ) and different grain sizes present through the thickness. Their tensile testing results indicated that the tensile strength and yield strength of joints increased and the elongation of joints decreased with increasing the tool rotary speed. They also measured Vickers micro-hardness across the joint at top, middle and bottom, and through the thickness in the WNZ. The result they got showed that the micro-hardness of different zones varied significantly. D. Venkateswarlu et al.[24], analyzed the friction stir welded joints of aluminum alloy 2219 in different heat-treated states. They used 2219-T87 and 2219-T62 to find the influence of base metal on characteristics of the joints. Their experimental output results exhibited that, mechanical properties, weld metal characteristics and joint failure locations are significantly affected by the different heat treatment conditions of the substrate. Prasanna et al.[25], used DEFORM-3D to perform finite element analysis and investigated experimentally to predict residual stress, temperatures, distortion of welded structure during FSW of an airframe structure made up of AA 2219 and AA 2014. They also developed a new technique of filling friction stir welding (FFSW) relying on a semi consumable joining tool to repair the keyhole left at the end of friction stir welding seam. Huijie Liu et al.[26], carried out friction stir welding of 2219-T6 aluminum alloy assisted by external non-rotational shoulder was carried out, and investigated the effects of the welding speed on microstructures and mechanical properties of 2219-T6. They showed that this new welding process is beneficial to improving the asymmetry and inhomogeneity, especially in the weld nugget zone. K. Surekha et al.[27], investigated the effect of processing parameters (rotation speed and traverse speed) on the corrosion behavior of friction stir processed high strength precipitation hardenable AA 2219-T87 alloy. The results indicated that the rotation speed has a major influence in determining the rate of corrosion, which is attributed to the breaking down and dissolution of the intermetallic particles. S. Arora et al.[28], used an adapted milling machine to friction stir weld aluminum alloy 2219 and found the effect of process parameters on the welding. The downward or forging force was found to be dependent upon shoulder diameter and rotational speed whereas longitudinal or welding force on welding speed and pin diameter. Tensile strength of welds was significantly affected by welding speed and shoulder diameter whereas welding speed strongly affected percentage elongation. Metallographic studies revealed fine equiaxed grains in weld nugget and micro-structural changes in thermo-mechanically affected zone were found to be the result of combined and interactive influences of frictional heat and deformation. R. Priya et al.[29], investigated the effect of post weld heat treatment on the microstructure and mechanical properties of dissimilar friction stir weldments of Al alloys 6061 and 2219 (in peak aged T6 temper). The survey of micro-hardness profile in the as-welded samples showed fluctuations across the weld zone and a minimum in the hardness occurred in the heat affected zone (HAZ) of alloy 6061. After a post weld ageing treatment at 165°C for 18h, the hardness was found to increase in weld zone alone and there is no effective improvement in HAZ hardness. On the other hand, a post weld solution treatment at 520°C followed by ageing at 165°C for 18h resulted in significant improvement in hardness across the whole weldment. M. Koilraj et al.[30] carried out the joining of dissimilar Al–Cu alloy AA2219-T87 and Al–Mg alloy AA5083-H321 plates using friction stir welding (FSW) technique and the process parameters were optimized using Taguchi L16 orthogonal design of experiments. The rotational speed, transverse speed, tool geometry and ratio between tool shoulder diameter and pin diameter were the parameters taken into consideration. The optimum process parameters were determined with reference to tensile strength of

the joint. The predicted optimal value of tensile strength was confirmed by conducting the confirmation run using optimum parameters. This study shows that defect free, high efficiency welded joints can be produced using a wide range of process parameters and recommends parameters for producing best joint tensile properties.

The literature survey concluded that a few researchers analyzed the FSW of aluminum AA6061-T6 plates. Therefore, this work aimed to develop a 3-D finite element heat transfer model for friction stir welding (FSW) of AA6061-T6. The numerical study was investigated the effects of tool traverse and rotational speed on thermal history.

II. Model Methodology

In this chapter, formulation is done for both heat generations in the shoulder and in the pin during Friction Stir welding.

Heat generation in flat cylindrical shoulder and cylindrical probe: Let us consider a cylindrical tool whose shoulder radius is R and radius of its probe is r_p whereas considering height of the probe as l as shown in Figure 1. It is considered that the angular speed of the tool is 'ω' and acted upon a plunging force P_n which generate a pressure 'P' on the shoulder surface, due to this pressure the total heat generation is calculated as follows.
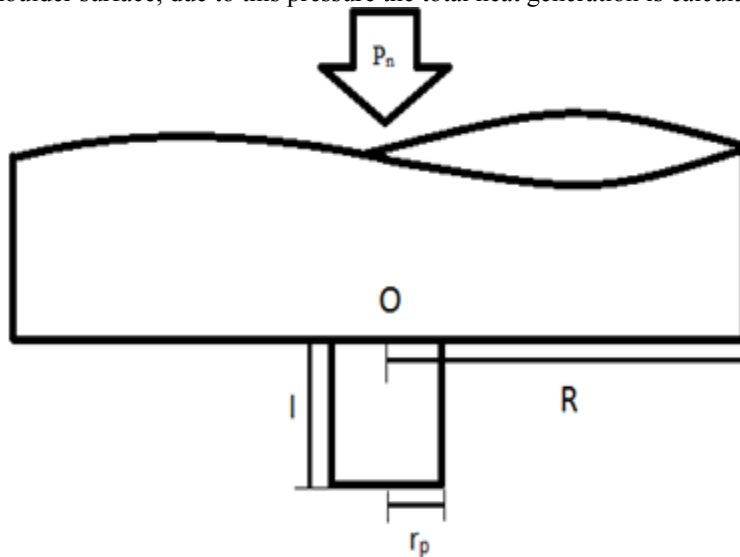
Figure 1: Schematic diagram of flat cylindrical shoulder and cylindrical probe**.**

Heat Generation in Shoulder: Taking an elemental ring of thickness 'δr' which is at r distance from the center 'O'

Therefore, the area of the elemental ring,

$$\delta A = 2\pi r \delta r \tag{1}$$
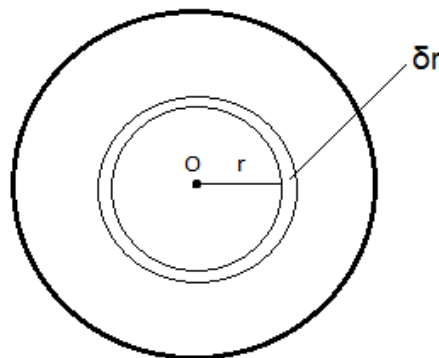
Figure 2: Small elementary area of the shoulder

Normal force acting due to this elemental ring,

$$\delta N = P \, . \, 2 \, \pi \, r \, \delta r \tag{2}$$

Let us take the frictional co-efficient between the tool and workpiece to be μ.
Therefore, Frictional force,

$$\delta F = 2 \, \mu \, P \pi \, r \, \delta r \tag{3}$$

Heat generation due to elemental ring,

$$\delta Q_{S1} = 2 \, \mu \, P \pi \, r \, \delta r \, . \, \omega r \tag{4}$$

Integrating both sides of eq. (4),

$$Q_{S1} = 2\mu\omega P\pi \int\limits_{r_p}^{R} r^2 \delta r$$

Or,
$$Q_{S1} = \frac{2}{3}\pi\mu\omega P(R^3 - r_p^3) \tag{5}$$

Heat generation in cylindrical probe
Similar to eq. (5),

$$Q_1 = \frac{2}{3}\pi\mu\omega P r_p^3 \tag{6}$$

Calculation of heat flux from cylindrical shoulder
Taking an elemental ring of thickness 'δr' at a distance r from the center O.
Therefore, the area of elemental ring, as shown in Fig. 2.

$$\delta A = 2\pi \, r \, \delta r \tag{7}$$

Normal force acting due to this elemental ring,

$$\delta N = P \, . \, 2 \, \pi \, r \, \delta r \tag{8}$$

Let us take the frictional co-efficient between the tool and workpiece to be μ.
Therefore, Frictional force,

$$\delta F = 2 \, \mu \, P \pi \, r \, \delta r \tag{9}$$

Heat generation due to elemental ring,

$$\delta Q_{S1} = 2 \, \mu \, P \pi \, r \, \delta r \times \omega r \tag{10}$$

Therefore, Heat flux (qs) can be obtained by dividing eq. (10) by (7), i.e.

$$\frac{\delta Q_{S1}}{\delta A} = \frac{2\mu P \pi r \delta r \times \omega r}{2\pi r \delta r} \tag{11}$$

Or,

$$q_S = \mu\omega P r \tag{12}$$

Net heat flux generated from cylindrical shoulder: The heat generated between the shoulder surface and the workpiece due to friction, a part of that heat is conducted in FSW tool itself due to the thermal conductivity of FSW tool[31]. Hence the fraction of heat flux ($q_s^{'}$) goes inside the workpiece is given as,

$$q_S^{'} = \frac{J_w}{J_w + J_t} q_S \tag{13}$$

where,

$$J = \sqrt{k\rho C_p} \tag{14}$$

The suffix w and t denote workpiece and tool. And k, ρ and Cp are the thermal conductivity, density and specific heat respectively.

Heat flux from tool pin: The volumetric heat flux (q_p) generating from the FSW tool pin is given by

$$q_p = \frac{\frac{2}{3}\pi\mu\omega \mathrm{Pr}_p^3}{\pi r_p^2 l}$$

(15)

III. Three-Dimensional Finite Element Model

A three-dimensional finite element transient thermal model was developed in the present work to analyze the heat transfer and temperature distribution in a FSW process. In the thermal model the actual conditions were accommodated as far as possible. The following assumptions were made in developing the present thermal model of a FSW process.

1. All the thermal properties were considered as function of temperature.
2. Linear Newtonian convection cooling was considered on all the surfaces.
3. Heat generation was considered as a load.
4. The interface heat loss was considered negligible.

The governing differential equation of conduction without heat generation is

$$\frac{\partial}{\partial x}[K\frac{dT}{dx}] + \frac{\partial}{\partial y}[K\frac{dT}{dy}] + \frac{\partial}{\partial z}[K\frac{dT}{dz}] = \rho C \frac{dT}{dt}$$

(16)

Where, ρ = density of plate material, C = specific heat and k = thermal conductivity. The following boundary conditions were applied in the present FE model.

Initial Boundary Condition

The initial temperature for the modeling that covers all the elements of the workpieces

$T = T_a$ for $t = 0$ (17)

Where, Ta is the atmospheric temperature for the present study. For boundary condition, a convective heat transfer coefficient 25 W/m^2°C for natural convection and ambient temperature 25°C were used for the thermal analysis. The mathematical expression for convection and radiation heat loss from the surfaces is given as:

(18)

$$K\frac{dT}{dn} = h(T - T_a) + \varepsilon\sigma(T^4 - T_a^4)$$

Where, n, h, ε and σ are the normal direction vector of the boundary, convection coefficient, emissivity and Stefan-Boltzmann constant respectively.

Heat source model: The heat input is linearly proportional to the distance from the center of the tool which is derived from the assumptions (a) the downward force applied to the workpiece from the tool creates a uniform pressure between the shoulder and the workpiece, and (b) the heat is generated from the work done by the friction force. The distribution of the rate of heat flux to work piece can then be represented as shown in equation,

(19)

$$q = \frac{3(Q_{S_1} + Q_1)r}{2\pi R^3} + \frac{Q_1}{\pi r^2 l}$$

Meshed model: In three-dimensional modeling DC3D8 or 8-node linear heat transfer brick element was employed. The total number of elements and nodes used in this modeling were 182880 and 208845 respectively. The workpiece was divided into three different mesh zones shown in Figure 3. In the central region up to 15 mm away from the welding line element size was kept fine with 1 mm in size while out of this zone, gradually increasing mesh was assigned.
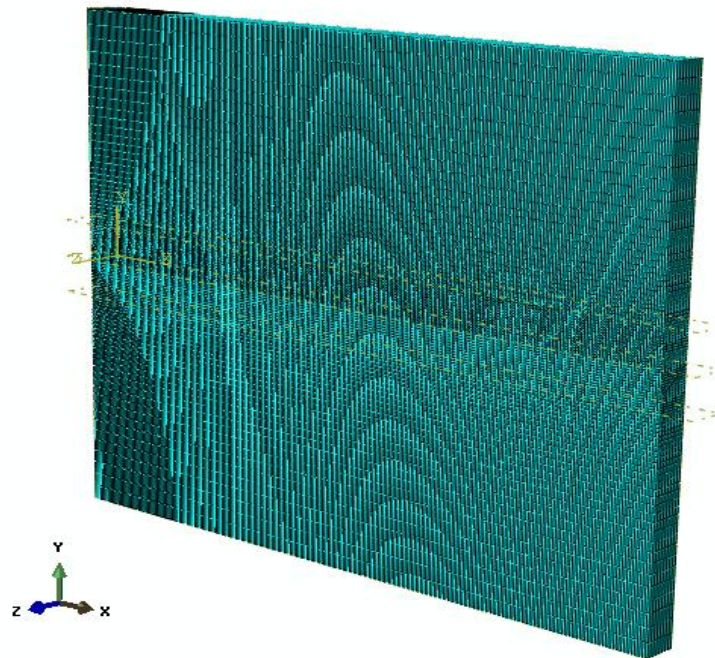
Figure 3: Meshed zone for FSW

Material properties: Figure 4 shows the temperature dependent material properties of AA 6061-T6 aluminum alloy[32] used for the transient heat transfer analysis. The chemical compositions of the aluminum alloy are shown in Table 1. For the bottom side of the plate constant convection co-efficient 300 W/m2°C was used in the analysis and for the remaining surfaces open to the air, it was taken as 25 W/m2°C. The ambient temperature was considered for numerical model as 25°C.
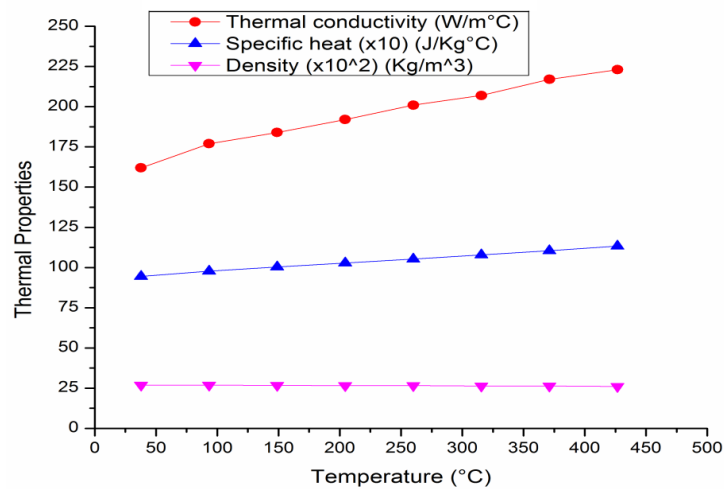
Figure 4: Thermal properties of AA 6061-T6

Table 1: Chemical composition of AA6061-T6 aluminum alloy[33]

Al	Cr	Cu	Fe	Mg	Mn	Si	Ti	Zn
95.8-98.6%	0.04-0.35%	0.15-0.4%	≤0.7%	0.8-1.2%	≤0.15%	0.4-0.8%	≤0.15%	≤0.25%

IV. Result and Discussion

In the present work, the three-dimensional finite element (FE) transient thermal numerical model was successfully validated with previously published journal of aluminium alloy 6061-T6[34]. The temperature dependent thermal properties of the material were considered to determine the transient temperature history. Newton's convection cooling was considered for the numerical analysis. To reduce the computation time, coarse mesh was assigned away from frictional heating region and finer mesh was assigned along and near the FSW zone.

Table 2: Process parameters for simulation of FSW process

Workpiece length (along x-coordinate)	254 mm
Workpiece half-width (along y-coordinate)	102 mm
Tool traverse speed	1.59 mm/s
Tool rotational speed	637 rpm

Tool geometry and dimensions: In this present study FE transient thermal analysis of FSW aluminum alloy 6061-T6 has been carried out by considering temperature dependent thermal material. The effects of tool geometry and process parameters were also considered in the thermal analysis. A cylindrical probe and flat shoulder tool have been used in this study. The detailed tool dimensions are given in Table 3.

Table 3: Tool dimensions

Material	Shoulder diameter	Probe diameter	Probe length
H-13	100 mm	12 mm	12 mm

Transient temperature profile: In this present FE model, validation of FSW numerical model was successfully validated against the previously published literature[34]. The process parameters for FSW were considered as given in the literature to model validation as shown in Table 4.

Table 4: Process Parameters obtained from the published literature

Thickness of the Plates (mm)	Rotational speed (rpm)	Traverse speed (mm/min)	Plunging force on FSW tool during welding (kN)
12.7	637	1.59	25
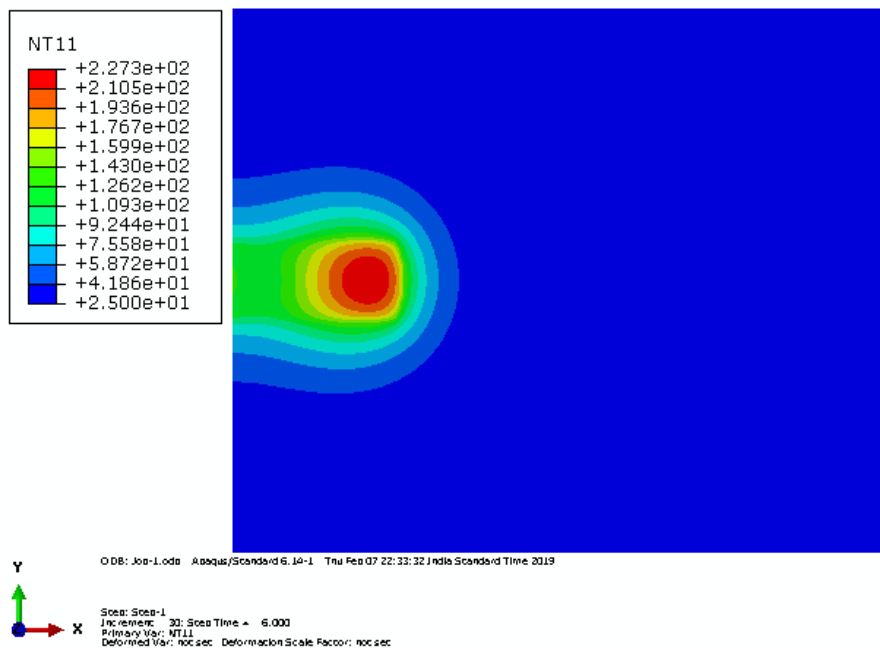
Figure 5: FE model for showing temperature analysis

The temperature contour of the top surface is shown in Figure 5. The model has been validated by comparing with published literature. From the combined thermal profiles, it was observed that published literature data is much closer to the simulated data as shown in Figure 6. It can be concluded that the present FE model can be successfully applied for the analysis of AA2219-T851 plates.
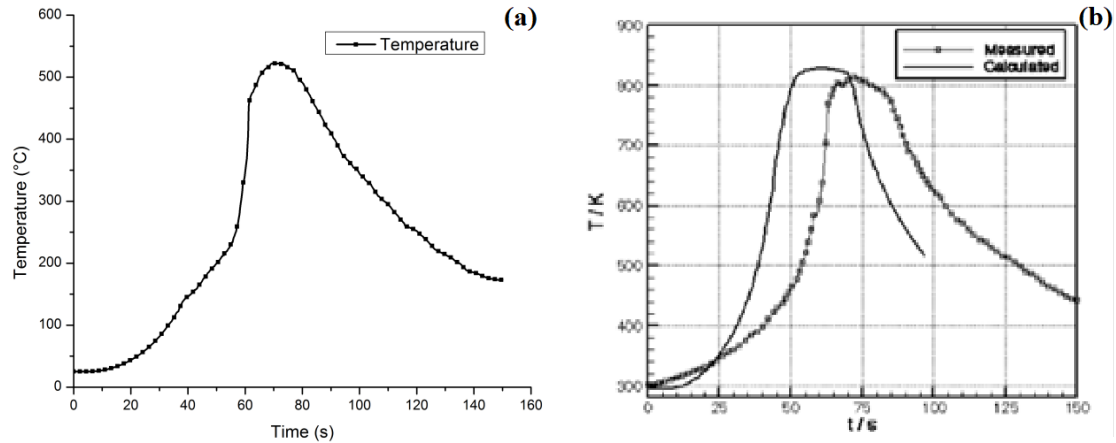
Figure 6: (a) Temperature distribution curve numerically calculated; (b) Temperature distribution curve obtained from the published paper.

Few simulations for AA2219-T851 were carried out on the Abaqus 6.14 to observe the effect of welding process parameters on transient temperature profiles as shown in Table 5.

Table 5: FSW Process parameters for AA2219-T851

Sl. No.	Process parameter for FSW		
	Rotational speed (RPM)	Traverse speed (mm/s)	Plunging force (kN)
1	450	1	7
2	450	2	7
3	450	3	7
4	600	1	7
5	600	2	7
6	600	3	7
7	750	1	7
8	750	2	7
9	750	3	7

The peak temperature of aluminum plates during FSW was increased with tool rotation speed. However, it decreased with increase in tool traverse speed as less contact time during high traverse speed which leads to less heat transfer between tool and the work piece as shown in Figs. (7-9).
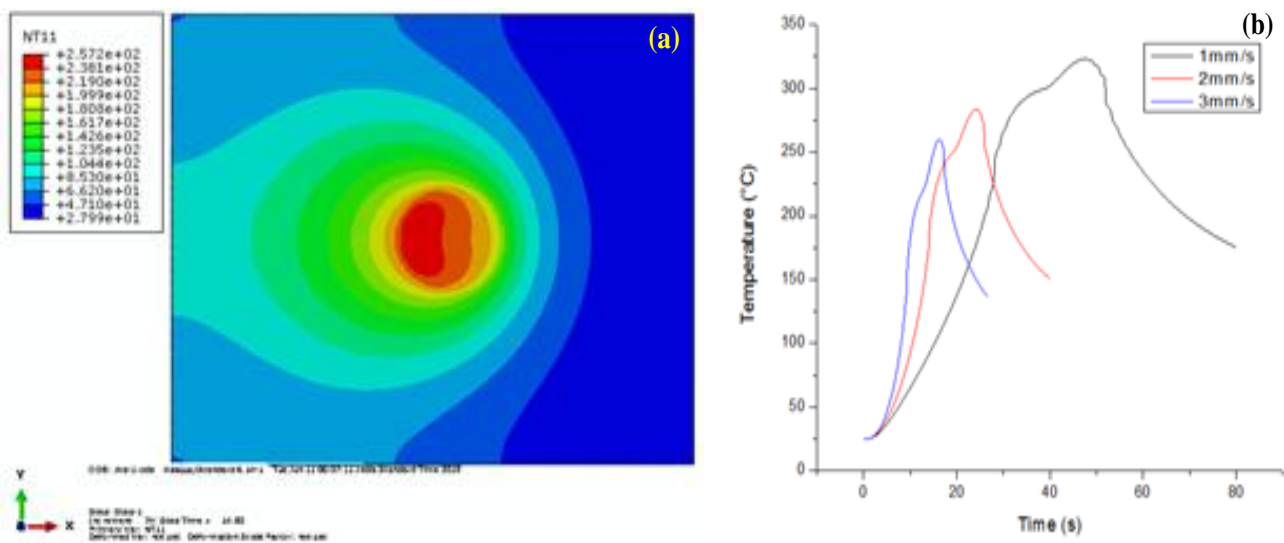
Figure 7: (a) Temperature contour at 450 rpm; (b) Temperature distribution curve at 450 rpm
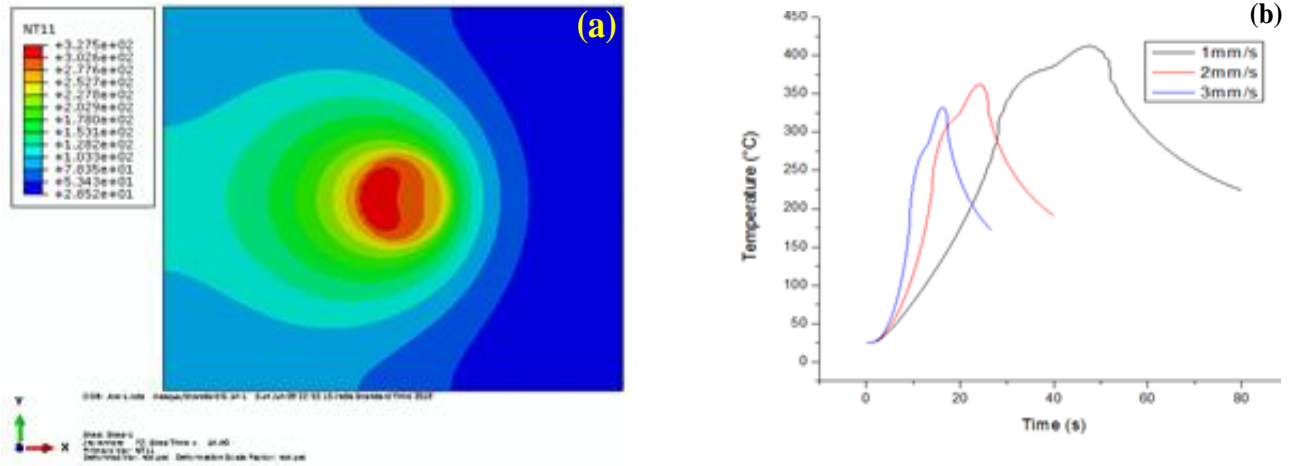
Figure 8: (a) Temperature contour at 600 rpm; (b) Temperature distribution curve at 600 rpm
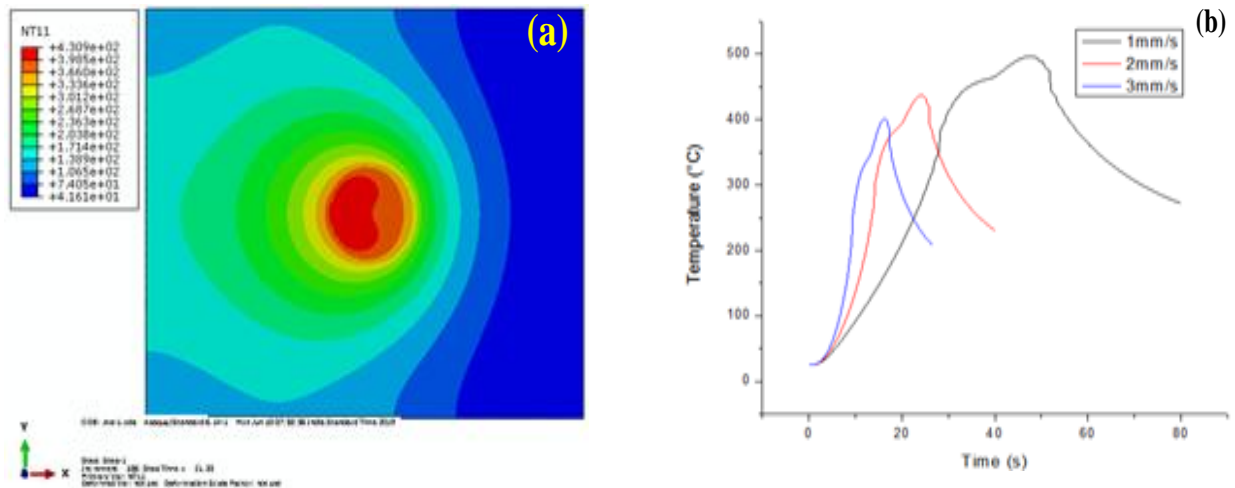
Figure 9: (a) Temperature contour at 750 rpm; (b) Temperature distribution curve at 750 rpm

V. Conclusion

In present study, the ABAQUS was used to simulate the welding plates. The major conclusions made from the analysis are:

> ➢ A finite element thermal model was successfully developed for friction stir welding of AA 6061-T6 plate.
> ➢ It was observed that peak temperature of aluminum plates decreased while increase in tool traverse speed.
> ➢ On increasing the tool rotational speed, the peak temperature increases.
> ➢ The maximum peak temperature achieved at 1 mm/s and 750 rpm of tool traverse speed and tool rotational speed respectively.

References

[1] Thomas, W. M., Nicholas, E. D., Needham, J. C., Murch, M. G., Temple-Smith, P., & Dawes, C. J. (1991). Friction stir butt welding, international patent application no. PCT/GB92 Patent application, (9125978.8).

[2] Bhadeshia, H. K. D. H. (2003). Joining of commercial aluminium alloys. In Proceedings of International Conference on Aluminium (INCAL'03), S. Subramanian and DH Sastry, Eds (pp. 195-204).

[3] Mishra, R. S., & Ma, Z. Y. (2005). Friction stir welding and processing. Materials science and engineering: R: reports, 50(1-2), 1-78.

[4] Threadgill, P. L., Leonard, A. J., Shercliff, H. R., & Withers, P. J. (2009). Friction stir welding of aluminium alloys. International Materials Reviews, 54(2), 49-93.

[5] Chao, Y. J., Liu, S., & Chien, C. H. (2008). Friction stir welding of al 6061- T6 thick plates: Part I- experimental analyses of thermal and mechanical phenomena. Journal of the Chinese institute of engineers, 31(5), 757-767

[6] Chen, K. E., Gan, W., Okamoto, K., Chung, K., & Wagoner, R. H. (2011). The mechanism of grain coarsening in friction-stir-welded AA5083 after heat treatment. Metallurgical and materials transactions A, 42(2), 488-507.

[7] Buffa, G., Ducato, A., & Fratini, L. (2011). Numerical procedure for residual stresses prediction in friction stir welding. Finite elements in analysis and design, 47(4), 470-476.

[8]   Gadakh, V. S., & Adepu, K. (2013). Heat generation model for taper cylindrical pin profile in FSW. Journal of Materials Research and Technology, 2(4), 370-375.
[9]   Fujii, H., Cui, L., Maeda, M., & Nogi, K. (2006). Effect of tool shape on mechanical properties and microstructure of friction stir welded aluminum alloys. Materials Science and Engineering: A, 419(1-2), 25-31.
[10]   Kumar, K. S. V. K., & Kailas, S. V. (2008). The role of friction stir welding tool on material flow and weld formation. Materials Science and Engineering: A, 485(1-2), 367-374
[11]   Zhao, Y. H., Lin, S. B., Qu, F. X., & Wu, L. (2006). Influence of pin geometry on material flow in friction stir welding process. Materials science and technology, 22(1), 45-50.
[12]   Zhang, Z., Liu, Y. L., & Chen, J. T. (2009). Effect of shoulder size on the temperature rise and the material deformation in friction stir welding. The International Journal of Advanced Manufacturing Technology, 45(9), 889-895.
[13]   Mehta, M., Arora, A., De, A., & DebRoy, T. (2011). Tool geometry for friction stir welding—optimum shoulder diameter. Metallurgical and Materials Transactions A, 42(9), 2716-2722.
[14]   Xu, S. W., Deng, X., Reynolds, A. P., & Seidel, T. U. (2001). Finite element simulation of material flow in friction stir welding. Science and Technology of Welding and Joining, 6(3), 191-193.
[15]   Santiago, D. H., Lombera, G., Urquiza, S., Cassanelli, A., & Vedia, L. A. D. (2004). Numerical modeling of welded joints by the" friction stir welding" process. Materials Research, 7(4), 569-574.
[16]   Cho, J. H., Boyce, D. E., & Dawson, P. R. (2007). Modelling of strain hardening during friction stir welding of stainless steel. Modelling and simulation in materials science and engineering, 15(5), 469.
[17]   Zhang, H. W., Zhang, Z., Jun, B. I. E., Lei, Z. H. O. U., & Chen, J. T. (2006). Effect of viscosity on material behavior in friction stir welding process. Transactions of Nonferrous Metals Society of China, 16(5), 1045-1052.
[18]   Ulysse, P. (2002). Three-dimensional modeling of the friction stir-welding process. International Journal of Machine Tools and Manufacture, 42(14), 1549-1557.
[19]   Nandan, R., Roy, G. G., & Debroy, T. (2006). Numerical simulation of three-dimensional heat transfer and plastic flow during friction stir welding. Metallurgical and materials transactions A, 37(4), 1247-1259.
[20]   Nandan, R. G. G. R., Roy, G. G., Lienert, T. J., & Debroy, T. (2007). Three-dimensional heat and material flow during friction stir welding of mild steel. Acta materialia, 55(3), 883-895.
[21]   Chen, Y., Liu, H., & Feng, J. (2006). Friction stir welding characteristics of different heat-treated-state 2219 aluminum alloy plates. Materials Science and Engineering: A, 420(1-2), 21-25.
[22]   Liu, H. J., Zhang, H. J., & Yu, L. (2011). Effect of welding speed on microstructures and mechanical properties of underwater friction stir welded 2219 aluminum alloy. Materials & Design, 32(3), 1548-1553.
[23]   Xu, W., Liu, J., Luan, G., & Dong, C. (2009). Temperature evolution, microstructure and mechanical properties of friction stir welded thick 2219-O aluminum alloy joints. Materials & Design, 30(6), 1886-1893.
[24]   Venkateswarlu, D., Cheepu, M., & Mahapatra, M. M. (2018, March). Analysing the Friction Stir Welded Joints of AA2219 Al-Cu Alloy in Different Heat-Treated-State. In IOP Conference Series: Materials Science and Engineering (Vol. 330, No. 1, p. 012074). IOP Publishing.
[25]   Prasanna, K. V. L., Reddy, P. S., & Murthy, N. G. (2017). Finite Element Simulation and Experimental Investigation of Friction Stir Welding of AA2219 and AA2014. IJSEAT, 5(9), 942-947.
[26]   Liu, H. J., Li, J. Q., & Duan, W. J. (2013). Friction stir welding characteristics of 2219-T6 aluminum alloy assisted by external non-rotational shoulder. The International Journal of Advanced Manufacturing Technology, 64(9), 1685-1694.
[27]   Surekha, K., Murty, B. S., & Rao, K. P. (2009). Effect of processing parameters on the corrosion behaviour of friction stir processed AA 2219 aluminum alloy. Solid state sciences, 11(4), 907-917.
[28]   Arora, K. S., Pandey, S., Schaper, M., & Kumar, R. (2010). Effect of process parameters on friction stir welding of aluminum alloy 2219-T87. The International Journal of Advanced Manufacturing Technology, 50(9), 941-952.
[29]   Priya, R., Sarma, V. S., & Rao, K. P. (2009). Effect of post weld heat treatment on the microstructure and tensile properties of dissimilar friction stir welded AA 2219 and AA 6061 alloys. Transactions of The Indian Institute of Metals, 62(1), 11-19.
[30]   Koilraj, M., Sundareswaran, V., Vijayan, S., & Rao, S. K. (2012). Friction stir welding of dissimilar aluminum alloys AA2219 to AA5083–Optimization of process parameters using Taguchi technique. Materials & Design, 42, 1-7.
[31]   Yang, Z. J., Zhao, X. H., Kou, H. C., Li, J. S., Rui, H. U., & Lian, Z. H. O. U. (2010). Numerical simulation of temperature distribution and heat transfer during solidification of titanium alloy ingots in vacuum arc remelting process. Transactions of Nonferrous Metals Society of China, 20(10), 1957-1962.
[32]   Awang, M., Mucino, V. H., Feng, Z., & David, S. A. (2005, April). Thermo-mechanical modeling of friction stir spot welding (FSSW) process: use of an explicit adaptive meshing scheme. In Technical Paper for the Society of Automotive Engineers 2005 World Congress.
[33]   http://asm.matweb.com/search/SpecificMaterial.asp?bassnum=ma6061t6
[34]   Song, M., & Kovacevic, R. (2003). Thermal modeling of friction stir welding in a moving coordinate system and its validation. International Journal of machine tools and manufacture, 43(6), 605-615.